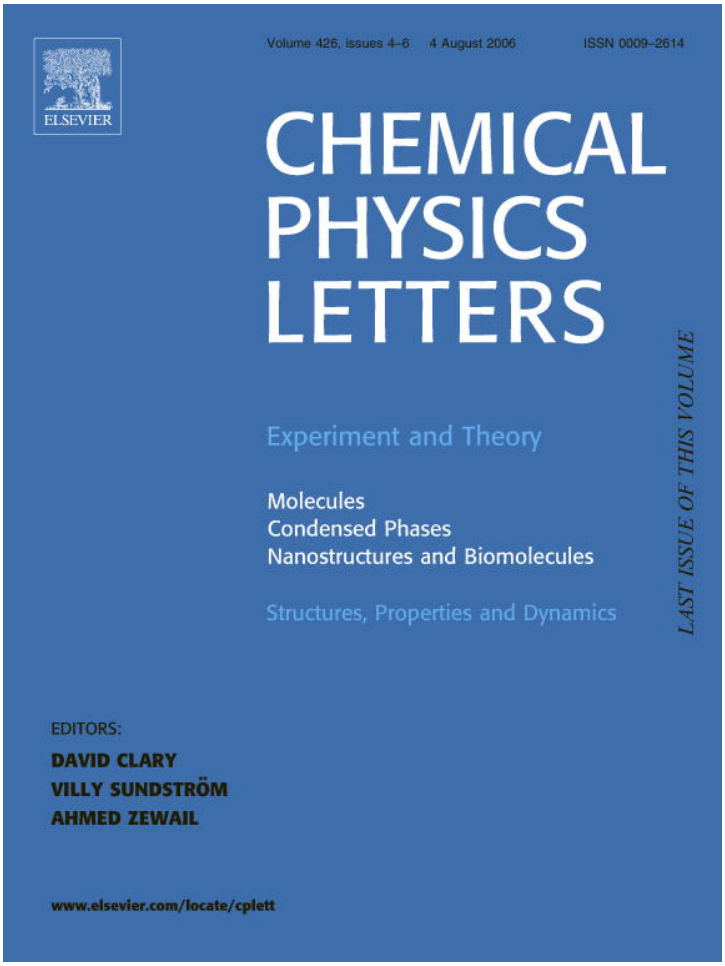

Available online at www.sciencedirect.com
SCIENCE DIRECT®
Chemical Physics Letters 426 (2006) 374–379
CHEMICAL PHYSICS LETTERS
www.elsevier.com/locate/cplett

First-principles calculations on the structural evolution of solid fullerene-like CP_x

G.K. Gueorguiev *, A. Furlan, H. Högberg, S. Stafström, L. Hultman

Department of Physics, IFM, Linköping University, S-581 83 Linköping, Sweden

Received 7 April 2006; in final form 22 May 2006
Available online 3 June 2006

Abstract

The formation and structural evolution of fullerene-like (FL) carbon phosphide (CP_x) during synthetic growth were studied by first-principles calculations. Geometry optimizations and comparison between the cohesive energies suggest stability for solid FL-CP_x compounds. In comparison with fullerene-like carbon nitride, higher curvature of the graphene sheets and higher density of cross-linkages between them is predicted and explained by the different electronic properties of P and N. Cage-like and onion-like structures, both containing tetragons, are found to be typical for fullerene-like CP_x. Segregation of P is predicted at fractions exceeding ~20 at.%.

1. Introduction

In the fullerene-like (FL) phases of carbon, the substitution of elements for C in graphene promotes layer bending and cross-linkage as in carbon nitride [1,2]. Such structure enables the material to extend the strength of a planar sp^2-coordinated carbon network in three dimensions [3]. C and N atoms share high electronegativity, low degree of polarizability, and similar distribution of the valence electrons which enables similar hybridization between their s and p electrons, i.e., sp, sp^2, and sp^3 bonding configurations. P can be viewed as an alternative dopant to N with similar valency, but lower electronegativity. Also noticeable is the phosphorus' preference for tetrahedral coordination. In its ground state, P does not have occupied d orbitals. Although the influence of d orbitals is usually overstated by simpler hybridization arguments, d-orbital hybridization (sp^3d) is invoked to explain the fact that P can form more than the usual number of bonds like in PF_5 and $POCl_3$. Since P shows a great variety of bonding configurations, also the possibilities of stable P fullerenes have been theoretically explored. Seifert et al. investigated different P fullerenes, compared them to C fullerenes, and found some pure P cage structures metastable [4]. All these features may lead to carbon phosphide (CP_x) compounds with new bonding features and promising technological properties.

C–P compounds have been produced as amorphous thin film material over a wide range of P:C composition ratios up to 3 [5]. Films with high P content usually show an amorphous structure. Typical for such films is a hydrogen content reaching 10% and their liability to oxidation [6]. In contrast, P-doped diamond-like carbon (P-DLC) films [7–9] have low P content which typically reaches 10–11 at.%. P-DLC thin films are electrically conducting at room temperature and exhibit significant mechanical hardness.

Pulsed laser ablation (PLA) offers an alternative route to produce pure C–P compounds in a H-free growth environment [9]. However, potential problems are likely to arise due to gas-phase condensation when super hot plume is expanded and cooled. The occurrence of stable P clusters such as P_4 and their trapping between graphene planes will put restrictions in the synthesis of compounds. A viable method to deposit FL-CP_x may be the reactive magnetron sputtering of the material in high or ultrahigh vacuum chambers which has been successfully used for deposition of well structured FL-CN_x, followed by the application of a capping layer (diffusion barrier).

* Corresponding author. Fax: +46 13 28 89 18.
E-mail address: gekos@ifm.liu.se (G.K. Gueorguiev).

0009-2614/$ - see front matter © 2006 Elsevier B.V. All rights reserved.
doi:10.1016/j.cplett.2006.05.087

Most of the theoretical studies up to date were dedicated to the polymorphs of the hypothetic C_3P_4 postulated together with the likewise hypothetic C_3N_4 as super-hard material [10,11]. FL-CP_x as a possible solid phase, however, has not been studied hither to.

By performing first-principles calculations on the FL-CP_x structural evolution, we aim to understand its potential stability, nano-structure, and growth mechanisms. Finite model systems in which P is incorporated in sp^2-hybridized graphene sheets are considered. The study involves both geometry optimizations and cohesive energy calculations performed within the framework of density functional theory (DFT) in its generalized gradient approximation (GGA). The CP_x growth evolution is understood as structural evolution during synthetic growth by sequential steps, where each step is defined by the previous relaxed structure. This theoretical approach was successfully applied to FL-CN_x [12,13] providing important findings about the role of the preformed CN species for the pentagon formation, the curvature of the graphene sheets, and the cross-linkages between them, as well as corroborating experimental observations of vapor-deposited FL-CN_x material. For the predictive qualities of the present work, our approach relies on ground state calculations and molecular modeling. However, we find in the FL-CP_x system several characteristic structures for which the energy gains are considerably larger than the thermal energy corresponding to typical deposition environments for FL compounds. Thus, our simulations are relevant when addressing vapor deposition situations. Also, we account for the precursor selection and for the competition between different pathways of structural evolution. In a previous work [14], we investigated the energetics of the preformed species C_nP_m ($1 \leqslant n, m \leqslant 3$) and P_n ($n \leqslant 4$), present in a CP_x film-forming flux, and the likeliness of different type of defects in CP_x graphene sheets. As a next natural step, the present work elaborates on the CP_x structure at larger scale, namely inter-layer cross-linkages, *onion-like* and *cage-like* structures. We find a higher density of cross-linkages and higher curvature of the graphene sheets in FL-CP_x compared to FL-CN_x for $x \leqslant 0.1$. At higher P content increasing amorphisation of CP_x becomes favorable. Segregation leading to P clustering inside the carbon matrix may play a significant role at $x \geqslant 0.2$.

2. Computational details

In a recursion model for the FL-CP_x structure evolution we optimize appropriate graphene CP_x clusters as initial growth templates. By adding sequences of incoming film-forming C_nP_m ($1 \leqslant n, m \leqslant 3$), P_n ($n \leqslant 4$) precursors, and free C and P atoms, we consider alternative growth paths to given relaxed curved and cross-linked structures. Differences in cohesive energies $|\Delta E_{coh}|$ for the possible structures are determined by an optimization strategy presented elsewhere [12,13].

The calculations were carried out using the GAUSSIAN 03 program [15] within the framework of DFT-GGA. For all results reported here, 6-31G* basis set (which is augmented with polarization functions) was employed. All numerical data presented and discussed in this work were obtained by making use of the B3LYP hybrid functional [16] which is known to provide an accurate description of the structural and electronic properties of fullerene-like thin films [12,13] and similar covalent systems [17–19].

In order to ensure that the results reported here do not depend on the level of theory chosen, test calculations employing also different basis sets (e.g., 6-311G(d)) and exchange correlation functionals (e.g., Perdew–Wang 91) have been performed. No significant differences with respect to the B3LYP/6-31G* results were found.

3. Results and discussion

3.1. Structural evolution of CP_x graphene sheets, cage-like features, and onion-like conformations

In a detailed first-principle investigation of the defects in FL-CP_x [14], we conclude that in contrast with the FL-CN_x the tetragon defects are energetically likely in CP_x. Due to the specific bonding nature of P as a third row element with low energy d-orbitals, it tends to form four-membered ring transition states. A study of the growth evolution near to a tetragon defect in FL-CP_x reveals some of its specific structural features. Fig. 1a shows an optimized model system $C_{15}PH_8$ containing a tetragon, together with the stable preformed species C_3P and C_2. Different combinations of precursors at different positions and orientations with respect to the template were considered, followed by geometry optimizations including rearrangements of the atomic positions. The chains of synthetic growth events in the environment of a tetragon defect lead to the following two results:

(i) P is stable within a graphene sheet. P-containing tetragons are also stable and do not break when more growth species (including additional P atoms) are added. During structural evolution close to an already existing tetragon defect, more P-containing tetragons may appear;
(ii) Cage-like structures typically result from different chains of synthetic growth which differ both in the type and sequence of precursors added; the only necessary condition being that the initial template is a tetragon-containing one. This trend is directly related to the tetrahedral bonding configuration preferred by P.

The most stable cage-like structure is shown in Fig. 1b. It corresponds to incorporation of C_3P and C_2 species and leads to a gain in E_{coh} of 0.77 eV (as compared to the initial system, Fig. 1a). A second P-containing tetragon forms by atomic rearrangements during optimization. A number of similar cage-like structures were obtained by adding of C_3P_2, C_2P, CP, C_2, P_2, and single atoms. The gain in E_{coh}

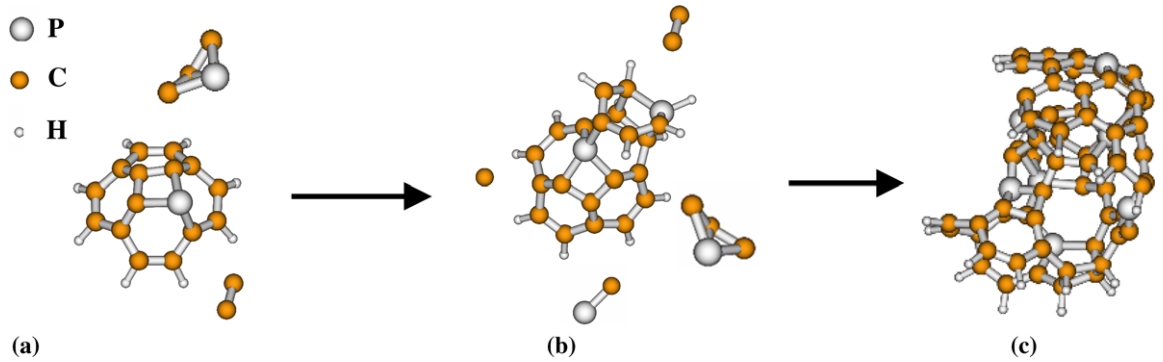

Fig. 1. (a) Model system for growth simulation consisting of a tetragon-containing template ($C_{15}PH_8$) and volatile species C_3P, C_2 (added in this sequence to obtain the cage-like structure in b); (b) The most stable ($C_{20}P_2H_{13}$) among the obtained cage-like conformations and precursors C, C_2, CP, and C_3P; (c) Further evolution of the system shown in (b) by successive addition of [C,C,C_3P,C,C], [C_2,C_2,C_2,C_2,C_3P], [C,C,C_2,C_2,C_2], [CP,C_3P,C,C,C_2], [C_2,C_2,C_2,C_3P,C], [C,C_2,C_2,C_2,C] resulting in an onion-like system ($C_{72}P_7H_{21}$).

for this family of structures varies between 0.35 and 0.7 eV depending on the number and the position of the additional P atoms. Consequently, the tetragon defect in CP_x is likely to prevail during synthetic growth. More remarkably, it can work as a seed for cage-like conformations and to generate further tetragons if more P-containing precursors are available.

The obtained curvature-effect due to P incorporation in graphene systems is in excellent agreement with the work of Melchor et al. [20] in which, at the same level of theory, the bonding of atomic P to graphene systems, hydrocarbons and fullerene cages was studied. The authors concluded that the bonding of P atoms both induces and enhances curvature in such structures.

The further evolution of the cage-shaped structure (Fig. 1b) is also investigated. By increasing the number of atoms in the system, the number of possible evolution 'channels' increases drastically. At these further growth steps our goal is not an unambiguous assigning of the energetically lowest system, but identifying probable evolution stages for the CP_x graphene shapes. In this case, a given structural development has to fulfill two criteria: (i) to bring a significant gain in $E_{coh} \geqslant 0.5$ eV. Nearly all studied evolution pathways bring gains in E_{coh} several times larger than the thermal energy at ambient temperature 0.025 eV or even at growth environment temperature 0.065 eV (which can be seen as a natural choice for a cut-off energy), but very few such chains of bonding events lead to a gain larger than 0.5 eV; and (ii) to result from more than one independent chain of synthetic growth.

The system shown in Fig. 1c can be described as an incomplete onion-like structure seeded by the initial tetragon defect. It is the most favorable in terms of E_{coh} (gain of 1.3 eV) among similarly sized structures resulting from that shown in Fig. 1b. The cage-like system in Fig. 1b and its analogues can be viewed as intermediate structures, generating additional tetragon defects which enhance the local curvature of the graphene sheets and disrupt two-dimensional growth. This conformation qualitatively differs from other structural features, such as curved sheets and 'bridge-like' cross-linkages relevant to both FL-CN_x [12,13] and FL-CP_x. The present results indicate that graphene sheets are expected to be considerably shorter and with higher curvature in FL-CP_x than in FL-CN_x, considering the same concentration of the doping element. We infer that onion-like features may be more frequent in FL-CP_x also at relatively low P content ($\leqslant$10 at.%) as judged by the stoichiometries of the structures shown in Fig. 1b and c. For FL-CN_x, onion structures favored by N incorporation were observed at twice the content of the dopant element (~21% N) with [21] or without [3] catalysts.

The mechanisms limiting the dopant content in FL-CP_x and FL-CN_x are different: the strong tendency to tetrahedral coordination of the electron-richer P atoms leads to amorphisation of CP_x whereas the high electronegativity of N and the strong triple bond in N_2 is related to the N_2 desorption from CN_x. In that context and following the organization of the Periodic Table (N, P, As, ... belong to its 15-th group), one can speculate that, if synthesizable, well-structured solid FL-CAs_x may not be able to accommodate more than ~5 at.% As.

3.2. Bond rotation due to an incorporated P atom and its structural implications for FL-CP_x

Another element of structure evolution is bond rotation. It gives rise to curved and cross-linked three-dimensional graphene bundles, as worked out first in CN_x [13]. The bond rotation in FL-CP_x is related to an incorporated P atom and the corresponding stabilization of pentagons.

A C atom was placed in the vicinity of the model template $C_{15}PH_9$. The as-formed C–C bond is aligned under different angles φ [0, 180°] and θ [0, 90°] to the axis $\boldsymbol{x}$ and to the plane $\boldsymbol{xy}$ of the template, as shown in Fig. 2a. The absolute value of the cohesive energy was then maximized with respect to [φ, θ] in order to determine the most favorable bond orientation. This procedure was repeated for a template with the P atom occupying a peripheral site (Fig. 2b) and for a pure C template ($C_{16}H_9$) interacting

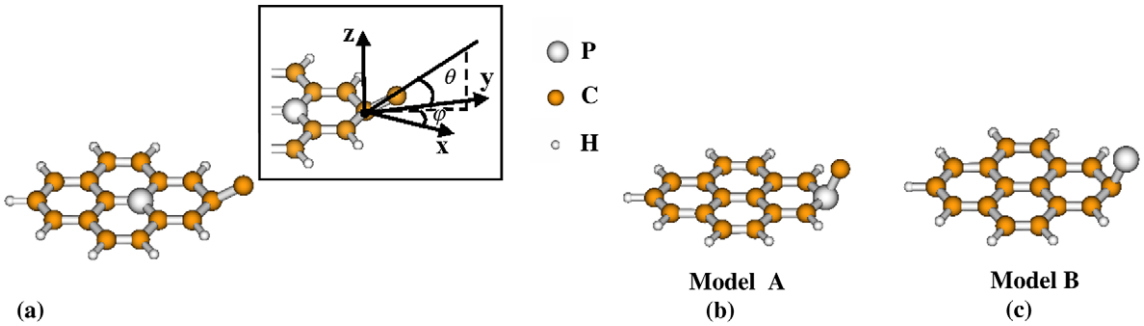

Fig. 2. Model templates illustrating bond rotation due to an incorporated P atom: (a) C atom added to $C_{15}PH_9$ with P at an internal site, (b) C atom added to $C_{15}PH_9$ with the P occupying a peripheral site (Model A), (c) $C_{16}H_9$ template, a P atom is added (Model B). Bond rotation angles are defined in the inset.

with a P ad-atom (Fig. 2c). In all three cases a bond rotation can take place, i.e., configurations with ($\theta \neq 0°$, $\varphi = 0°$) are locally stable. When the P atom is at an internal site (Fig. 2a), however, the planar configuration without bond rotation ($\theta = 0°$, $\varphi = 0°$) is with 0.75 eV more favorable than that with a bond rotation. Bond rotation is favorable for bonds between a P atom at a peripheral site and a C ad-atom or vice-versa. In the systems illustrated in Fig. 2b,c, the structures with a bond rotation of ($\theta \approx 70°$, $\varphi = 0°$), labeled Model A and Model B, respectively, are more stable than their planar isomers with 0.16 eV and 0.1 eV, respectively. The cohesive energies corresponding to isomeric systems with and without bond rotation are displayed in Table 1. The stability obtained for structures with a bond rotation is considerably less pronounced than in FL-CN_x. This has two implications:

(i) The cross-linking mechanism initiated by a bond rotation found to exist in FL-CN_x, should be less frequent in CP_x;
(ii) During synthetic growth, a significant rearrangement of the local geometry in the vicinity of a bond rotation site can take place.

The model templates which include a non-planar bond (Fig. 2b,c) were used as starting points for simulations to verify if such a rotated bond can serve as a cross-linkage site between graphene sheets. By attaching selections of relevant species [14]; C, P, C_3P, C_2P, CP, and P_2 in subsequent steps, each one followed by geometry optimizations, it was possible to compare different intermediate structural alternatives. Only the most stable configuration obtained at a given step among the different ad-species and the most favorable positions of the P atoms are considered. The P incorporation rate was kept below 10–15 at.% P.

Fig. 3a, b, show curved and cross-linked curved structures, respectively, resulting from typical chains of growth events starting with Model A. The growth evolution starting from Model B leads to similar, but less stable (by 0.3–0.4 eV) structures. The cohesive energy data related to Fig. 3, listed in Table 2, show that both curved graphene layers without cross-linkage and similar systems with a 'bridge-like' cross-linking may appear as a result of the incorporation of single P atoms as well as CP dimers, and subsequent pentagon formation. However, larger gain in E_{coh} was obtained for growth chains, in which precursors containing more than one P atom, i.e., CP_2, and/or pure species like P_2 were added to the growth template. Such reaction sequence resulting in a stable structure $C_{27}P_5H_{18}$ is shown in Fig. 3c. The gain in E_{coh} for the sequence in Fig. 3c is 0.54 eV (i.e., by ~0.35 eV more than that in Fig. 3b). Again, it contains tetragons instead of pentagons, and the cross-linkage site is 'branched', apparently creating conditions for an 'inter-link' of three graphene layers (see the inset in Fig. 3c). Further attachment of precursors to the three branches of this 'inter-link' (the curved layer, the hexagon synthesized on the right side, and the CP-bridge on the left side) is energetically favorable, strongly disrupting the layered graphene network of the material in the vicinity of the inter-link site and leading to branched, densely intersected graphene layers. This suggests that inter-link sites can prevail becoming seeds for

Table 1
B3LYP cohesive energies corresponding to the finite systems displayed in Fig. 2a, b, and c

Structure	$C_{15}PH_9$ + C P at internal site		$C_{15}PH_9$ + C P at peripheral site (Model A)		$C_{16}H_9$ + P (Model B)	
θ bond rotation (deg.)	0	36 (31)	0	68 (62)	0	70 (62)
E_{coh} (eV)	4.32 (4.62)	3.57 (4.19)	5.06 (5.73)	5.22 (6.01)	4.78 (5.21)	4.88(5.42)
ΔE_{coh} (eV)	−0.75 (−0.43)		0.16 (0.28)		0.1 (0.21)	

For each system, the cohesive energies are tabulated for its planar isomer and the most stable isomer with bond rotation. The last row represents the cohesive energy differences between these isomers ($\Delta E_{coh} = E_{coh}(\theta \neq 0°) - E_{coh}(\theta = 0°)$). The B3LYP E_{coh} values corresponding to the analogous CN_x systems are listed in parentheses (data taken from [12]).

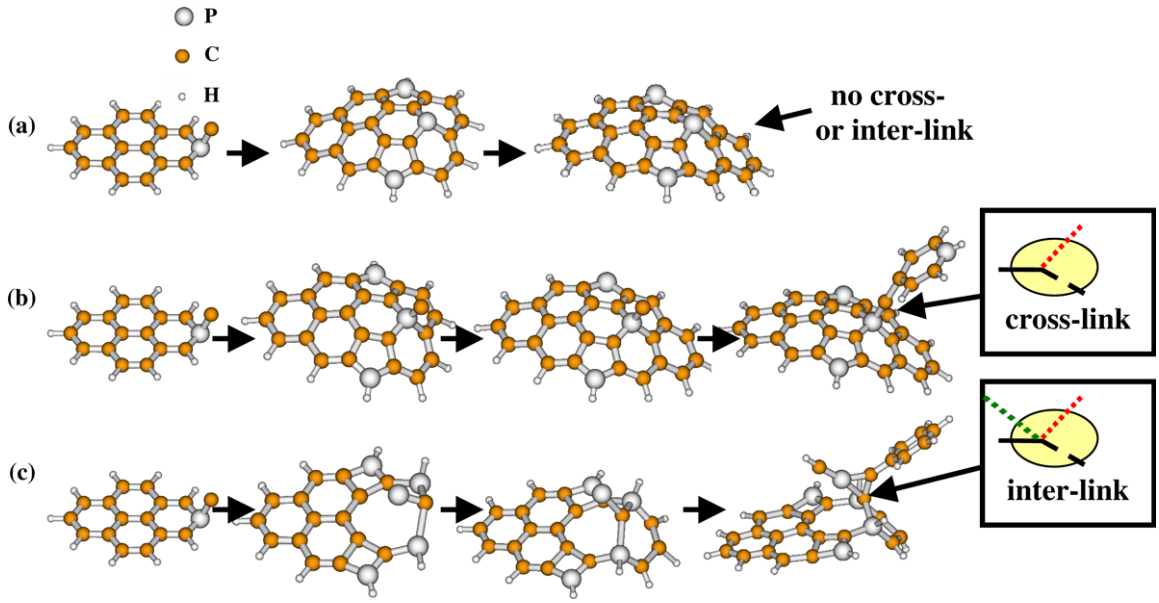

Fig. 3. Most competitive chains of bonding events during synthetic growth of CP_x, starting from Model A in Fig. 2: (a) two pentagon defects separated by a hexagon in a curved system $C_{25}P_3H_{12}$ without cross/inter-linkage; (b) reaction sequence ending up with a cross-linked system, $C_{31}P_4H_{17}$; (c) reaction chain resulting in an inter-linked system containing tetragons (schematically shown in the inset).

Table 2
B3LYP cohesive energies corresponding to the model systems at each step of the reaction schemes shown in Fig. 3

Chain in Fig. 3a				
Stoichiometry	$C_{16}PH_9$	$C_{22}P_3H_{11}$	$C_{25}P_3H_{12}$	–
θ cross-link (deg.)	68	no cross-link	no Cross-link	–
E_{coh} (eV)	5.22	5.30	5.33	–
ΔE_{coh} (eV)	0	0.08	0.11	–
Chain in Fig. 3b				
Stoichiometry	$C_{16}PH_9$	$C_{23}P_3H_{11}$	$C_{26}P_3H_{11}$	$C_{31}P_4H_{17}$
θ cross-link (deg.)	68	92	92	100
E_{coh} (eV)	5.22	5.30	5.34	5.38
ΔE_{coh} (eV)	0	0.08	0.12	0.16
Chain in Fig. 3c				
Stoichiometry	$C_{16}PH_9$	$C_{16}P_5H_9$	$C_{19}P_5H_{12}$	$C_{27}P_5H_{18}$
θ cross-link (deg.)	68	–	–	inter-link
E_{coh} (eV)	5.22	5.35	5.59	5.76
ΔE_{coh} (eV)	0	0.13	0.37	0.54

The angles of rotation θ of the cross-linking bond are also listed. ΔE_{coh} represents the cohesive energy gain as compared to the initial step which for all chains is $C_{16}PH_9$ (Model A).

three-dimensional locally amorphous structures due to closely intersected and branched atomic layers.

Although the diversity of feasible precursors and alternative structures at each growth step is too large for an exhaustive study, two features of our approach contribute to a better sampling of the corresponding potential energy hypersurface: (i) randomly chosen atoms in already relaxed structures are moved out from their equilibrium positions and made subjects of structure re-optimizations; and (ii) given final systems, e.g., those in Fig. 3, are obtained by more than one chain of incorporation events differing in the sequence of the individual precursors added.

3.3. Segregation

In a separate set of optimizations, systems with larger content (up to 30 at.%) of P at substitutional sites were investigated. It is found that CP_x layers can accommodate P contents up to ~25% by distributing the P atoms and defect formation. This occurs by breaking P–P bonds and promoting new C–P bonds. The convergence of two-dimensional structures becomes increasingly difficult with increasing P content while E_{coh} decreases to <1 eV. Fig. 4a shows the converged system with the highest P content. It has $E_{coh} = 0.92$ eV which is a considerably lower value compared to the cohesive energies listed in Tables 1 and 2 that varied between 3.57 and 5.76 eV. CP_x systems with P content exceeding ~20% tend to have disrupted sheet geometry and form amorphous three-dimensional structures with P segregation. Especially, the incorporation of relatively large precursors (such as pure P_4 or mixed species like C_3P_2, both containing P–P bonds, Fig. 4b) creates P-rich areas in the system. Structures in which most of the P atoms are bonded together become energetically more favorable, i.e., less P atoms remain bonded only to carbons.

The most favorable case ($E_{coh} = 1.44$ eV) within a family of conformations with segregation is shown in Fig. 4c. When only one individual P_4 species is added to a pure graphene sheet or a sheet with low P content (e.g., $\leqslant$5–10 at.%), the P atoms from that P_4 can still intermix with carbons at the site of incorporation. This means that at low P content, a mechanism of an individual P_4 dissociation and incorporation eventually leading to defect formation (tetragons, pentagons, cross-linkages) prevails and no segregation takes place.

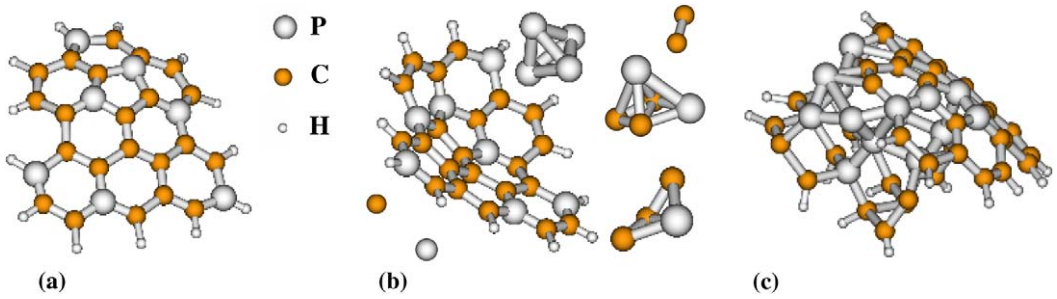

Fig. 4. Sheet-geometry of high P content system: (a) initial optimized structure ($C_{22}P_7H_{13}$); (b) the same system undergoing incorporation of P-rich species indicated in the figure; and (c) energetically favorable relaxed system ($C_{42}P_{15}H_{19}$), exhibiting segregation, obtained from (b) after incorporation of the precursor species indicated.

4. Conclusions

Chains of synthetic growth events of FL-CP_x were studied and different competing geometries at each step of the structure evolution were compared taking into account C_nP_m ($1 \leqslant n$, $m \leqslant 3$), P_n ($n \leqslant 4$) precursors for the growth process. Due to the P low energy d-orbitals, P-containing tetragon defects are stable and prevail when more growth species are added to the template. Thus, tetragons play an important role for buckling of the FL-CP_x graphene sheets and also serve as nucleation centers of characteristic FL-CP_x conformations, in the form of cage-like and onion-like structures, as were recently experimentally observed in FL-CN_x. Tetragons in CP_x may induce the formation of additional tetragons in their vicinity by bonds/atomic positions rearrangement during further addition of P-containing precursors. Pentagon defects can also form in FL-CP_x mostly when smaller precursors such as single atoms and C_2, CP dimers prevail among the added species. However, pentagon defects in FL-CP_x are by 0.7–1 eV less favorable than in FL-CN_x. When a P atom is incorporated in a graphene sheet, rotation of a CP bond near the incorporation site is promoted, which results in buckling of the graphene sheet by pentagon(s) and/or tetragon(s) formation and cross- as well as inter-linking between sheets. Overall, due to the P bonding nature and the type of the predominating defects, FL-CP_x exhibits shorter and stronger curved graphene sheets than its CN_x counterpart. Well-structured FL-CP_x thin films are expected for P content $\leqslant$10 at.%. For higher concentrations, CP_x becomes increasingly amorphous and if the P content exceeds 20–25 at.%, clustering and segregation of P become energetically increasingly favorable. These results set an upper limit for the P concentration in FL-CP_x. It is worth to be noted, that disruption of FL-CP_x structure happens at roughly twice lower content of the dopant element (20 at.% P) than for FL-CN_x (>35 at.% N).

Acknowledgements

The research was supported by The Swedish Foundation for Strategic Research (SSF) Strategic Research Centre on Materials Science for Nanoscale Surface Engineering (MS^2E) and the European Commission. The National Supercomputer Center in Linköping is gratefully acknowledged for providing high performance computing resources.

References

[1] H. Sjöström, M. Boman, S. Stafström, J.-E. Sundgren, Phys. Rev. Lett. 75 (1995) 1336.
[2] L. Hultman, J. Neidhardt, N. Hellgren, H. Sjöström, J.-E. Sundgren, MRS Bull. 28 (2003) 19.
[3] J. Neidhardt, Zs. Czigány, I.F. Brunell, L. Hultman, J. Appl. Phys. 93 (2003) 3002.
[4] G. Seifert, T. Heine, P.W. Fowler, Eur. Phys. J. D 16 (2001) 341.
[5] S.R.J. Pearce, P.W. May, R.K. Wild, K.R. Hallam, P.J. Heard, Diam. Relat. Mater. 11 (2002) 1041.
[6] F. Claeyssens, G.M. Fuge, N.L. Allan, P.W. May, S.R.J. Pearce, M.N.R. Ashfold, Appl. Phys. A 79 (2004) 1237.
[7] V.S. Veerasamy, G.A.J. Amaratunga, C.A. Davis, A.E. Timbs, W.I. Milne, D.R. McKenzie, J. Phys.: Condens. Mater 5 (1993) L169.
[8] A. Helmbold, P. Hammer, J.U. Thiele, K. Rohwer, D. Meissner, Philos. Mag. B72 (1995) 335.
[9] G.M. Fuge, P.W. May, K.N. Rosser, S.R.J. Pearce, M.N.R. Ashfold, Diam. Relat. Mater. 13 (2004) 1442.
[10] J.-C. Zheng, M.C. Payne, Y.P. Feng, A.T.-L. Lim, Phys. Rev. B 67 (2003) 153105.
[11] F. Claeyssens, J.M. Oliva, P.W. May, N.L. Allan, Int. J. Quantum Chem. 95 (2003) 546.
[12] G.K. Gueorguiev, J. Neidhardt, S. Stafström, L. Hultman, Chem. Phys. Lett. 401 (2005) 288.
[13] G.K. Gueorguiev, J. Neidhardt, S. Stafström, L. Hultman, Chem. Phys. Lett. 410 (2005) 228.
[14] A. Furlan, G.K. Gueorguiev, H. Högberg, S. Stafström, L. Hultman, Thin Solid Films, accepted for publication.
[15] M.J. Frisch, Gaussian Inc., Wallingford, CT, 2003.
[16] A.D. Becke, J. Chem. Phys. 98 (1993) 5648.
[17] S. Stafström, L. Hultman, N. Hellgren, Chem. Phys. Lett. 340 (2001) 227.
[18] R.-H. Xie, G.W. Bryant, V.H. Smith Jr., Chem. Phys. Lett. 368 (2003) 486.
[19] R.-H. Xie, G.W. Bryant, L. Jensen, J. Zhao, V.H. Smith Jr., J. Chem. Phys. 118 (2003) 8621.
[20] S. Melchor, J.A. Dobado, J.A. Larsson, J.C. Greer, J. Am. Chem. Soc. 125 (2003) 2301.
[21] C. He, N. Zhao, C. Shi, X. Du, J. Li, L. Cui, F. He, Scripta Mater. 54 (2006) 1739.